

## Elastic continuum analysis of the liquid crystal polarization grating

Ravi K. Komanduri and Michael J. Escuti\*

*Department of Electrical and Computer Engineering, North Carolina State University, Raleigh, North Carolina 27695, USA*

(Received 30 December 2006; published 8 August 2007)

We apply elastic continuum theory to model critical parameters influencing the free-energy equilibrium configuration and the dynamic performance of a continuous and in-plane liquid crystal profile acting as a polarization grating. We present analytical expressions for the threshold voltage, critical thickness, and the dynamic switching times under strong anchoring conditions, negligible flow, and arbitrary splay, twist, and bend constants. We also study the influence of weak anchoring, and derive expressions describing a dramatic reduction of the critical thickness and voltage threshold, even for modest grating periods and surface anchoring strengths. Good correlation exists with previously reported experimental data, except in the dynamic response; we therefore show that flow effects (backflow and kickback) likely play an essential role in the fall times, presumably due to the prominent splay-bend deformation of the zero-field configuration. We consider the impact of surface pretilt, and validate our entire analysis with numerical simulations. The approximation technique we employ is likely broadly useful for many problems which include nano- or micropatterned surfaces.

DOI: [10.1103/PhysRevE.76.021701](https://doi.org/10.1103/PhysRevE.76.021701)

PACS number(s): 61.30.Dk, 42.79.Kr, 42.79.Dj, 61.30.Hn

### I. INTRODUCTION

Liquid crystal gratings (both bulk and polymer-dispersed) have received significant attention due to their potential to act as switchable diffractive optical elements. Recently, a continuous and periodic configuration of a nematic liquid crystal (LC), shown in Fig. 1, was proposed [1,2] as a compelling way to implement polarization gratings (PGs). This general class of diffractive optics [3–5] is embodied by periodic, spatially varying, optically anisotropic profiles, including both birefringence and dichroism. Many unique and useful diffractive properties have been identified and considered for applications in displays [6,7], diffractive optics [4,5], optical storage [8,9], and polarimetry [10,11]. One structure in particular is the focus of this work (Fig. 1), and is known as a liquid crystal polarization grating (LCPG). In recent work [7,12–14], we have shown that the LCPG structure may be experimentally realized with effectively ideal optical properties using photoalignment materials in combination with polarization holography, completely overcoming the LC defects and optical scattering prominent in initial experimental efforts.

The nominal LCPG profile illustrated in Fig. 1(a) results from boundaries that establish a nematic director  $\mathbf{n}$  at the surfaces ( $z = \pm d/2$ ) that follow

$$\mathbf{n}(x) = \cos(\pi x/\Lambda)\mathbf{x} + \sin(\pi x/\Lambda)\mathbf{y} + 0\mathbf{z}, \quad (1)$$

where  $\Lambda$  is the effective optical grating period (note that the true nematic grating period is  $2\Lambda$ ).

It was realized early that the stable director configuration will not be uniformly in-plane for arbitrary cell gap thicknesses  $d$  or in the presence of a strong electric field. In fact, a critical thickness  $d_C$  was theoretically identified [2,15,16] below which the director will match Eq. (1), and above which the director will spontaneously distort out-of-plane.

When an electric field is applied perpendicular to the substrates, the nematic director is also expected to reorient out-of-plane as illustrated in Fig. 1(b). A Freedericksz voltage threshold  $V_{th}$  was identified [1,16] with values similar to other display modes. Previous analyses employ the one-constant approximation [1,15], which remains inaccurate, and does not characterize realistic device behavior. Moreover, dynamics were completely overlooked even though it is well understood for other LC modes [17,22].

We seek to better understand the equilibrium and dynamic behavior of the LCPG, with as few assumptions as possible (arbitrary elastic constants). We will arrive at a coupled variational problem, unlike that predicted by the one-constant approximation. To simplify and decouple this system, we propose an equivalent model for the LCPG that is general enough to accurately identify key device parameters, yet simple enough to solve analytically. We then consider pretilt and weak anchoring. Comparisons to numerical simulations and published experimental work are included wherever possible. This rigorous analysis addresses why experimental realization of defect-free LCPGs has been unexpectedly challenging, and predicts the material parameters and geometry that should optimize fabrication.

### II. ELASTIC CONTINUUM MODEL

The general expression of the Frank-Oseen elastic energy density ([17], Chap. 2) for nonchiral nematic LCs in the absence of electromagnetic fields is

$$\omega_F = \frac{1}{2}K_1(\nabla \cdot \mathbf{n})^2 + \frac{1}{2}K_2(\mathbf{n} \cdot \nabla \times \mathbf{n})^2 + \frac{1}{2}K_3(\mathbf{n} \times \nabla \times \mathbf{n})^2 + \frac{1}{2}K_2 \nabla \cdot [(\mathbf{n} \cdot \nabla)\mathbf{n} - (\nabla \cdot \mathbf{n})\mathbf{n}], \quad (2)$$

where  $K_1$ ,  $K_2$ , and  $K_3$  are the elastic constants corresponding to splay, twist, and bend deformations, respectively. When an

\*mjescuti@ncsu.edu

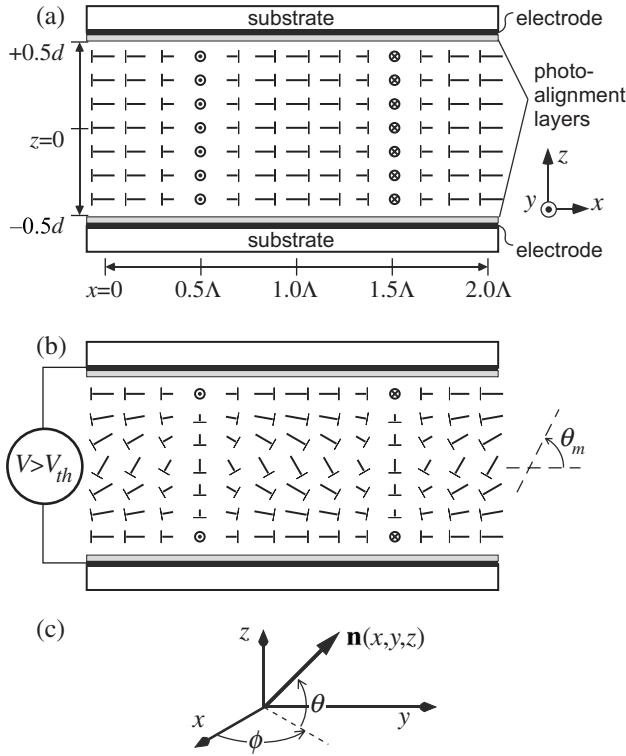


FIG. 1. (a) LCPG geometry. (b) Distorted LC configuration when  $V > V_{th}$ . (c) Definition of nematic director  $\mathbf{n}$ .

applied electric field  $\mathbf{E}$  is present, the electric energy density can be expressed as

$$\omega_{elec} = -\frac{1}{2}\epsilon_0\Delta\epsilon(\mathbf{n} \cdot \mathbf{E})^2, \quad (3)$$

where  $\epsilon_0$  is the vacuum permittivity and  $\Delta\epsilon$  is the dielectric anisotropy of the LC.

The local average orientation of LC molecules, defining the nematic director  $\mathbf{n}$ , can generically be written as a unit-vector field using the geometry of Fig. 1(c),

$$\mathbf{n}(\theta, \phi) = \cos\theta \cos\phi \mathbf{x} + \cos\theta \sin\phi \mathbf{y} + \sin\theta \mathbf{z}, \quad (4)$$

where  $\theta$  and  $\phi$  are the tilt and azimuth angle, respectively. In our case,  $\theta(x, z)$ ,  $\phi(x, z)$ , and  $\mathbf{n}(x, z)$  are all independent of  $y$  due to the geometry of our boundaries.

We can estimate equilibrium electro-optical properties by finding the lowest-energy nematic director profile using variational minimization given the spatial boundary conditions and external electric field ([17], Chap. 3). We now refer to the LCPG geometry shown in Fig. 1 and make the following clarifying assumptions: (i) Strong anchoring conditions exist ensuring that  $\theta=0$  and  $\phi=\pi x/\Lambda$  at  $z=\pm d/2$ . In Sec. V we relax this condition and consider weak anchoring. (ii) We define  $\theta \equiv \theta(z)$  and  $\phi \equiv \phi(x)$ . Since this holds for the ideal zero-field configuration [Fig. 1(a)], we anticipate that it is also valid for low fields. (iii) The electric field is along the  $z$  axis and generated by an applied voltage such that  $E=|\mathbf{E}|=V/d$ . (iv) When  $V > V_{th}$ , we assume the tilt angle is symmetric about the center of the sample,  $\theta(z)=\theta(-z)$ . (v) The

maximum tilt angle  $\theta_m$  at any equilibrium state occurs at the center of the sample,  $\theta(z=0)=\theta_m$  and  $\partial\theta/\partial z|_{z=0}=0$ .

Using these, the bulk elastic energy density ( $\omega=\omega_F+\omega_{elec}$ ) can be simplified to

$$\omega = f(\theta, \phi) \left( \frac{\partial\phi}{\partial x} \right)^2 + g(\theta) \left( \frac{\partial\theta}{\partial z} \right)^2 + h(\theta, \phi) \left( \frac{\partial\phi}{\partial x} \right) \left( \frac{\partial\theta}{\partial z} \right) - \frac{1}{2}\epsilon_0\Delta\epsilon E^2 \sin^2\theta, \quad (5a)$$

$$f(\theta, \phi) = \frac{\cos^2\theta}{2} [K_2 \sin^2\theta + K_3 \cos^2\theta + e(\theta, \phi)], \quad (5b)$$

$$e(\theta, \phi) = \sin^2\phi (K_1 - K_2 \sin^2\theta - K_3 \cos^2\theta), \quad (5c)$$

$$g(\theta) = \frac{1}{2} (K_1 \cos^2\theta + K_3 \sin^2\theta), \quad (5d)$$

$$h(\theta, \phi) = (K_2 - K_1) \cos^2\theta \sin\phi. \quad (5e)$$

Using the classic variational approach ([17], Chap. 2), nematic director configurations with minimum free-energy density must be solutions to

$$\frac{\partial}{\partial x} \left( \frac{\partial\omega}{\partial\phi_x} \right) - \frac{\partial\omega}{\partial\phi} = 0, \quad (6a)$$

$$\frac{\partial}{\partial z} \left( \frac{\partial\omega}{\partial\theta_z} \right) - \frac{\partial\omega}{\partial\theta} = 0, \quad (6b)$$

where “ $x$ ” and “ $z$ ” refer to partial derivatives with respect to  $x$  and  $z$ , respectively. A system of coupled differential equations results:

$$\frac{\partial}{\partial x} \left( 2f(\theta, \phi) \frac{\partial\phi}{\partial x} \right) - \frac{\partial f(\theta, \phi)}{\partial\phi} \left( \frac{\partial\phi}{\partial x} \right)^2 = 0, \quad (7a)$$

$$\frac{\partial}{\partial z} \left( 2g(\theta) \frac{\partial\theta}{\partial z} \right) - \frac{\partial f(\theta, \phi)}{\partial\theta} \left( \frac{\partial\phi}{\partial x} \right)^2 - \frac{\partial g(\theta)}{\partial\theta} \left( \frac{\partial\theta}{\partial z} \right)^2 + \epsilon_0\Delta\epsilon E^2 \sin\theta \cos\theta = 0. \quad (7b)$$

These constitute a system of coupled nonlinear second order differential equations. The coupling arises primarily through the term  $f(\theta, \phi)$ , which generally has nonconstant partial derivatives to both  $\theta$  and  $\phi$  variables. Solutions to Eqs. (7) therefore necessarily lead to  $\theta(x, z)$  and  $\phi(x, z)$ , functions that depend on both spatial variables. Because our initial assumption used to derive Eqs. (7) was that  $\theta$  and  $\phi$  were independent, this contradiction means that we ought to rederive the total energy density [Eqs. (5)], leading to more complicated expressions which cannot be solved analytically. Note that the one-constant approximation completely neglects this coupling.

We instead suggest a different approximation to Eq. (5b) which allows for analytical solutions to be found for its essential equilibrium and dynamic properties that are nearly identical to those of the original problem. We will test the validity of the resulting analytic expressions using an inde-

pendent numerical approach to the original problem. The approximation is as follows: since  $\sin^2\phi$  is bounded by 0 and 1, we introduce a parameter  $\alpha \rightarrow 0 < \alpha < 1$  so that  $f(\theta, \phi)$  no longer depends on  $\phi$ :

$$f(\theta, \phi) \rightarrow \hat{f}(\theta) = \frac{\cos^2\theta}{2} [K_2 \sin^2\theta + K_3 \cos^2\theta + \alpha(K_1 - K_2 \sin^2\theta - K_3 \cos^2\theta)]. \quad (8)$$

Using this new expression, Eqs. (7) are now transformed to equations that can now be solved analytically:

$$\frac{\partial^2\phi}{\partial x^2} = 0, \quad (9a)$$

$$\frac{\partial}{\partial\theta} \left[ g(\theta) \left( \frac{\partial\theta}{\partial z} \right)^2 \right] - \frac{\partial\hat{f}(\theta)}{\partial\theta} \left( \frac{\partial\phi}{\partial x} \right)^2 + \epsilon_0\Delta\epsilon E^2 \sin\theta \cos\theta = 0. \quad (9b)$$

Even though this model no longer completely describes the original situation, as will be later shown, it is sufficient to identify the critical device inflection points (voltage threshold and critical thickness). Since  $\alpha=0$  and  $\alpha=1$  to give the bounds for these equilibrium parameters. By comparing to numerical simulation which models the original problem, we find this to be true and furthermore find a particular value of  $\alpha$  that accurately estimates each of those parameters for all LC materials considered. The numerical simulation is performed with LC3D (Liquid Crystal Display 3-D Director Simulator Software), a modeling package [19] which solves for nematic director configurations given material parameters (including arbitrary elastic constants) and boundary conditions, under the assumptions of strong anchoring, no-flow, and a constant order parameter.

Solutions to Eqs. (9) can be found by applying the classical reasoning used to find Freedericksz-type transitions. Using the boundary condition [Eq. (1)], we can identify that  $\phi = \pi x/\Lambda$  is the solution to Eq. (9a). One obvious “undistorted” solution to Eq. (9b) is  $\theta(z)=0$ . We can furthermore find “distorted” solutions ([17], Chap. 3) to find the implicit relationship between  $\theta$  and  $z$ ,  $d$ , and  $E$ :

$$\frac{\pi}{\Lambda} \left( z + \frac{d}{2} \right) = \int_0^{\beta(z)} G(\theta_m, \beta) d\beta, \quad (10a)$$

$$G(\theta_m, \beta) = [K_1 + (K_3 - K_1)\sin^2\theta_m \sin^2\beta]^{1/2} \{ \alpha K_1 + (1 - \alpha) \times [2K_3 - K_2 + \sin^2\theta_m(1 + \sin^2\beta)(K_2 - K_3)] + \epsilon_0\Delta\epsilon E^2 (\Lambda/\pi)^2 \}^{-1/2} (1 - \sin^2\theta_m \sin^2\beta)^{-1/2}, \quad (10b)$$

$$\beta(z) = \sin^{-1} \left( \frac{\sin\theta(z)}{\sin\theta_m} \right). \quad (10c)$$

Solutions to Eq. (10) describe the equilibrium state of the LCPG for any given grating geometry, elastic constants, and electric field. We will use them to analyze the transition be-

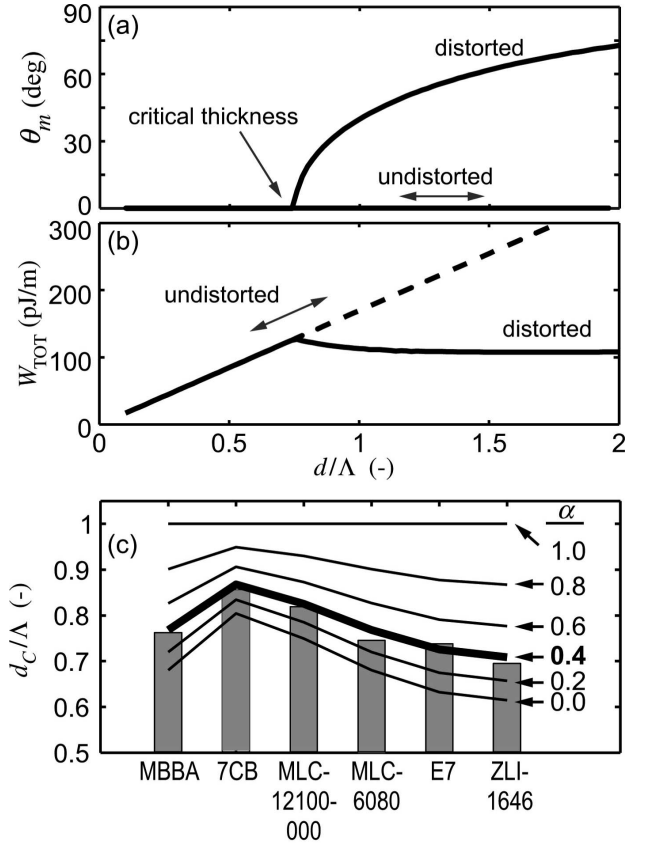


FIG. 2. (a) Calculated maximum tilt angle  $\theta_m$  for nematic MLC-6080 (and  $\alpha=0.4$ ), showing the critical thickness  $d_c$ . (b) Total energy  $W_{TOT}$  for both potential solutions. (c) Comparison of  $d_c$  for various LC materials (Merck [20,22]) analytically calculated using Eq. (10) as a function of  $\alpha$  and numerically calculated with LC3D (bars). The solution  $\alpha=0.4$  gives the best match.

tween the two configurations in Fig. 1, and derive the critical thickness and voltage threshold in Secs. III A and III B, respectively. Subsequently in Sec. III C, we will apply the Ericksen-Leslie dynamic equations to model the switching behavior.

### III. STRONG ANCHORING CONDITIONS

#### A. Critical thickness

As with almost all LC pixel structures, the cell thickness  $d$  is a key design parameter affecting both the optical and electro-optical behavior of the device. In the LCPG, the thickness takes on a unique role. If we solve Eqs. (10) for the thicknesses that produce a maximum tilt angle  $\theta_m$  when no field is present ( $E=0$ ), we identify the distorted solutions. These distorted angles and the undistorted solution are plotted in Fig. 2(a) for the nematic MLC-6080 ( $\Delta\epsilon=+7.2$ ,  $[K_1, K_2, K_3]=[14.4, 7.1, 19.1]$  pN, Ref. [20]). Note that the thickness solution corresponding to  $\theta_m=0$  in Eqs. (10) leads to the critical thickness

$$d_C(\alpha) = \Lambda \left[ \alpha + (1 - \alpha) \left( \frac{2K_3}{K_1} - \frac{K_2}{K_1} \right) \right]^{-1/2}, \quad (11)$$

that identifies the point at which the distorted solution appears. In order to identify which configuration has the lower total energy  $W_{TOT}$  when  $d > d_C$ , we solve Eq. (10) to find  $\theta(z)$  for each solution  $\theta_m$  and then integrate the energy density [Eqs. (5), with Eq. (8)] to find the total energy. As shown in Fig. 2(b), the distorted configuration clearly has a lower total energy above the critical thickness, and is therefore the preferred solution.

We now determine the best value of the so-far undetermined  $\alpha$ . Since  $K_2 \leq K_1 \leq K_3$  in most LCs, the lower and upper bound for  $d_C$  occurs as  $\alpha=0$  and  $\alpha=1$ :

$$\frac{\Lambda}{\sqrt{\frac{2K_3}{K_1} - \frac{K_2}{K_1}}} \leq d_C \leq \Lambda. \quad (12)$$

In Fig. 2(c), we use Eq. (11) to calculate  $d_C$  as  $\alpha$  is varied from 0 to 1 for various nematic LC materials. We also use LC3D to numerically calculate the critical thickness for these same materials. When superimposed in Fig. 2(c), it is clear that  $\alpha=0.4$  in the analytical equation predicts the numerical data best. One explanation of  $\alpha$  is that it averages out the  $x$  dependence of  $\theta$  across the entire period of the grating. We might then expect that  $\langle \sin^2(\pi x/\Lambda) \rangle = 0.5$  is the best value of  $\alpha$ , but due to the nonlinear nature of the problem, it is different.

The  $d_C$  reported using a completely different numerical technique [15] also correspond well, supporting our assertion that the analytical expression for  $d_C$  in Eq. (11) is reasonable, in spite of the approximation [Eq. (8)]. Substituting  $K_3=K_1$  in the lower bound for  $d_C$  gives the two-constant approximation expression derived earlier [16]. The one-constant approximation gives the less accurate estimate  $d_C=\Lambda$  calculated previously [2,15].

Since the desired in-plane LC configuration of Fig. 1(a) contains only splay and bend deformations, the critical thickness may be intuitively understood as the point beyond which the introduction of a twist deformation becomes energetically favorable. It may also be thought of as maximum thickness for which the interaction length of the two surfaces dominate the behavior of the bulk.

### B. Voltage threshold

The effect of an external electric field on the LCPG cell (assuming  $d < d_C$ ) can be described as a Freederickz transition. Below a certain voltage threshold  $V_{th}$  [1,16], the LC configuration remains unaffected. Once the voltage exceeds the threshold value, the lowest energy configuration is distorted. Using the same process as with the critical thickness (but now with  $E=V/d \neq 0$ ) we can identify the voltage threshold as

$$V_{th} = \pi \sqrt{\frac{K_1}{\epsilon_0 \Delta \epsilon}} \left[ 1 - \left( \frac{d}{d_C} \right)^2 \right]^{1/2}, \quad (13)$$

where  $\Delta \epsilon$  is the dielectric anisotropy and  $d_C$  is the critical thickness identified in Eq. (11). In Fig. 3 we compare  $V_{th}$

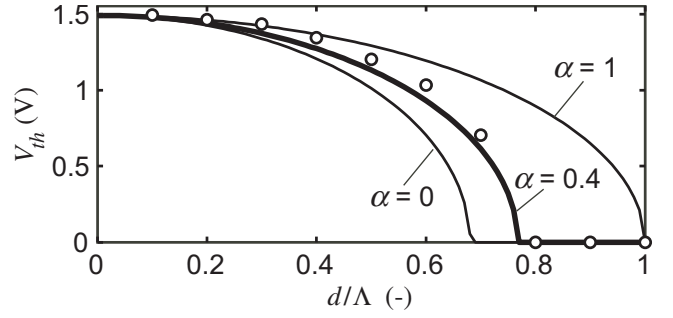


FIG. 3. Threshold voltage  $V_{th}$  for the material MLC-6080 analytically calculated (curves) using Eq. (13) and numerically calculated (circles) using LC3D.

analytically calculated for MLC-6080 to values numerically simulated using LC3D. As expected, the numerically simulated results fall between the analytical bounds, with  $\alpha=0.4$  as the best fit.

Note that  $V_{th}$  approaches the value  $\pi \sqrt{K_1/\epsilon_0 \Delta \epsilon}$  for small  $d/\Lambda$ , indicating that this threshold approaches the well-known value ([17], Chap. 3) for a homogeneously aligned cell. As previously identified [1], the voltage threshold vanishes as  $d$  approaches  $d_C$ . However, this should also be understood in light of the existence of the critical thickness (which effectively means that when  $d \geq d_C$  the grating is already switched). The earlier one-constant approximation [1] can also be verified.

### C. Switching times

In order to estimate the dynamic response times resulting from a step-input change in the electric field, we turn to the Ericksen-Leslie dynamic equations ([17], Chap. 4). We will assume a no-slip condition (i.e., local fluid velocity is zero everywhere) in this discussion, even though we suspect *a priori* that this is a rough approximation (since backflow and kickback effects are usually prominent in the case of splay and bend geometries [18]). It nevertheless allows us to find no-flow analytic expressions that can be compared to numerical results from LC3D as well as experimental results, and be used to show that flow does in fact play a significant role.

The dynamic director configuration must satisfy

$$\frac{\partial}{\partial z} \left( \frac{\partial \omega}{\partial \theta, z} \right) - \frac{\partial \omega}{\partial \theta} - \gamma_1 \frac{\partial \theta}{\partial t} = 0, \quad (14)$$

where  $\gamma_1$  is the rotational viscosity. After applying the energy density expressions derived in Sec. II [including Eq. (8) with the parameter  $\alpha$ ], we find

$$\gamma_1 \frac{\partial \theta}{\partial t} = \frac{\partial}{\partial \theta} \left[ g(\theta) \left( \frac{\partial \theta}{\partial z} \right)^2 - \hat{f}(\theta) \left( \frac{\pi}{\Lambda} \right)^2 \right] + \epsilon_0 \Delta \epsilon E^2 \sin \theta \cos \theta. \quad (15)$$

This expression does not have an analytic solution in general (to our best efforts). Therefore we make the conjecture that the term  $\partial g(\theta)/\partial \theta (\partial \theta/\partial z)^2$  is negligible, and subsequently check this with the full numerical solutions obtained

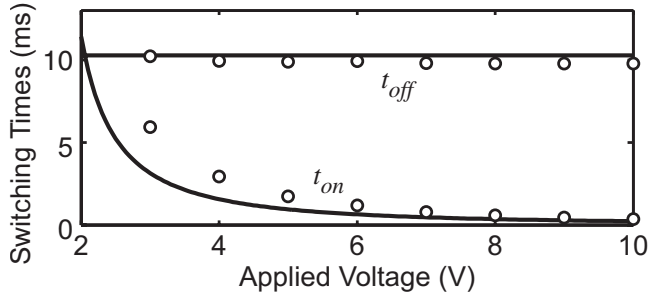


FIG. 4. No-flow rise ( $t_{on}$ ) and fall ( $t_{off}$ ) times for MLC-6080 analytically calculated (curves) using Eq. (18) and numerically calculated (circles) using LC3D ( $d=2 \mu\text{m}$ ,  $\Lambda=11 \mu\text{m}$ ).

from LC3D simulation. In fact, this is exactly true if  $K_1=K_3$ , as was done in a previous work [16]. Therefore after neglecting this term and using ( $\sin \theta \approx \theta$ ), the tilt angle must follow

$$\gamma_1 \frac{\partial \theta}{\partial t} = K_1 \frac{\partial^2 \theta}{\partial z^2} + \theta \left[ K_1 \left( \frac{\pi}{d_C} \right)^2 + \epsilon_0 \Delta \epsilon E^2 \right]. \quad (16)$$

Using the ansatz ([17], Chap. 5)

$$\theta(z, t) = \sum_{k=1}^{\infty} A_k \cos\left(\frac{k\pi z}{d}\right) \exp\left(-\frac{t}{\tau_k}\right), \quad (17)$$

we can identify the  $\tau_k$  exponential time constants that describe the director response when a field is suddenly applied. As with many display modes, the switch-ON time dynamics are bounded by  $\tau_{on} = -\tau_{k=1}$ . In a similar manner, the switch-OFF time constant  $\tau_{off}$ , when a field is suddenly removed, can be identified when  $E=0$  in Eq. (16). These no-flow response times are

$$\tau_{on} = \frac{\gamma_1 d^2}{\epsilon_0 \Delta \epsilon (V^2 - V_{th}^2)}, \quad (18a)$$

$$\tau_{off} = \frac{\gamma_1 d^2}{\epsilon_0 \Delta \epsilon V_{th}^2}, \quad (18b)$$

where  $V_{th}$  was defined earlier. These are related to the 10–90% rise time  $t_{on}$  and 90–10% fall time  $t_{off}$  measured in experiments through  $t_{on} = \ln(9)\tau_{on}$  and  $t_{off} = \ln(9)\tau_{off}$ , respectively.

As a representative case, in Fig. 4 we compare these analytic rise and fall times developed using the no-flow assumption with those calculated numerically using LC3D for the material MLC-6080 ( $\gamma_1=157 \text{ mPa s}$ , Ref. [20]). Strong correlation can be seen in this example (and with all other LC parameters we simulated), primarily because the LC3D also neglects all flow effects [19].

While these two simulations concur well with each other, the fall times from experiment are five to six times faster [12–14]. This suggests that backflow (and perhaps kickback) effects are dominant in the LCPG due to the strong bend and splay deformations, and should be theoretically included as an effective viscosity (Ref. [17], Chap. 5). However, in the

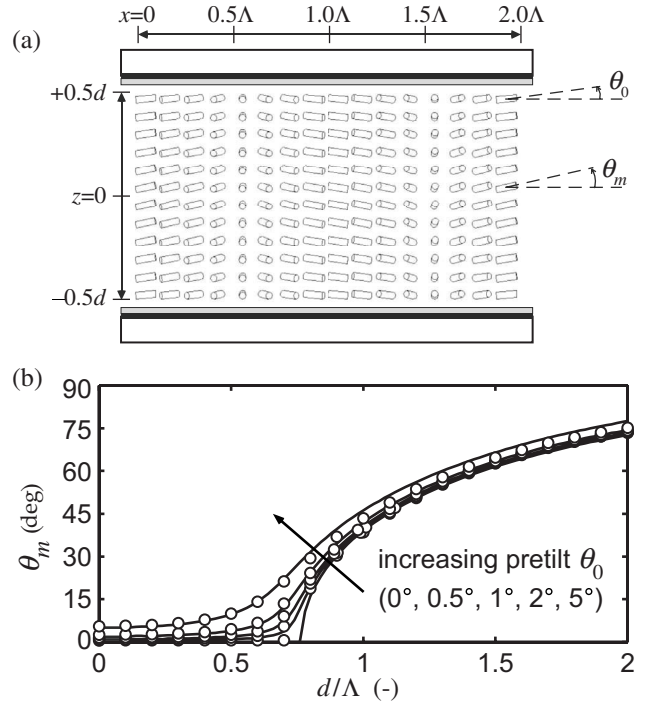


FIG. 5. (a) LCPG nematic director with a nonzero pretilt  $\theta_0 = 5^\circ$  and  $d/\Lambda=0.5$ , predicted by LC3D. (b) Maximum tilt angle  $\theta_m$  for MLC-6080 analytically calculated using Eq. (19) (curves) and numerically calculated using LC3D (circles).

case of the LCPG flow effects cannot be analyzed even with the approximations made so far and hence is beyond our present scope.

#### IV. EFFECT OF PRETILT

In the discussion thus far, a zero pretilt has been assumed in order to simplify the analysis as much as possible. Now we seek to understand if those results are still applicable when a small, nonzero pretilt exists. Pretilts are usually essential to LC devices because they provide a nondegenerate reference that assists in avoiding disclinations and instabilities arising from a zero-pretilt symmetry [21]. We show in Fig. 5(a) the LCPG configuration found with LC3D when a nonzero pretilt  $\theta_0=5^\circ$  is applied with strong anchoring conditions (compare to Fig. 1). By again applying the assumptions in Sec. II, we find that a modified Eq. (10a) can be used to understand the dependence of  $d_C$  and  $V_{th}$  on  $\theta_0$ :

$$\frac{\pi d}{\Lambda 2} = \int_{\beta_0}^{\pi/2} G(\theta_m, \beta) d\beta, \quad (19a)$$

$$\beta_0 = \sin^{-1} \left( \frac{\sin \theta_0}{\sin \theta_m} \right). \quad (19b)$$

As in the zero-pretilt case, the transition between undistorted and distorted solutions occurs when we set  $\theta_m = \theta_0$  in Eq. (19). Since this leads to  $\beta_0 \rightarrow \pi/2$ , the integral vanishes, and both Freedericksz-type transitions occur when  $d_C=0$  and

$V_{th}=0$ . However, when the pretilt is small ( $0 < \theta_0 \ll 1$ ), the two solutions are not substantially different (i.e.,  $\theta_m$  remains nearly  $\theta_0$ ) until the thickness approaches  $d_C$  or the applied voltage approaches  $V_{th}$ . Similar to the effect of pretilt in standard display modes (Ref. [17], Chap. 3), we can quantify this distortion by defining  $\theta_m = \theta_0 + \delta$ , where the deformation  $|\delta| \ll 1$ . By substituting this into Eq. (19) and rearranging, we can find how  $\delta$  depends on thickness (when  $E=V/d=0$ ) and on applied voltage (with fixed  $d < d_C$ ), respectively:

$$\delta \approx \theta_0 \left[ \sec\left(\frac{\pi d}{2 d_C}\right) - 1 \right], \quad (20a)$$

$$\delta \approx \theta_0 \left[ \sec\left(\frac{\pi}{2} \sqrt{1 + (V^2 - V_{th}^2) \frac{\epsilon_0 \Delta \epsilon}{\pi^2 K_1}}\right) - 1 \right], \quad (20b)$$

where  $d_C$  and  $V_{th}$  refer to the strong anchoring values derived earlier. Note that both deformations are nearly zero until  $d$  and  $V$  approach  $d_C$  and  $V_{th}$ , respectively.

Figure 5(b) shows the maximum tilt angle analytically determined using Eq. (19) and numerically calculated using LC3D. Note the strong correspondence between the two, and that both confirm our analytical reasoning that the thresholds predicted for  $\theta_0=0^\circ$  sufficient to characterize the LCPG for small pretilt values.

## V. WEAK ANCHORING CONDITIONS

Weak anchoring conditions permit surface director reorientation in response to electromagnetic fields and/or pixel geometry. Since weak anchoring strengths of photoalignment materials are well known [21,23,24], it is important to understand its effect on the critical thickness and voltage threshold. This may also help explain the difficulty [1,25,26] in experimental fabrication of LCPGs without defects until recently [7,12–14].

The surface anchoring energy density [27] applied to our periodic geometry (and zero pretilt) is given by

$$\omega_s = W_p \sin^2 \theta + W_a \cos^2 \theta \sin^2\left(\phi - \frac{\pi x}{\Lambda}\right), \quad (21)$$

which depends on a polar (or tilt) energy strength  $W_p$  and an azimuthal energy strength  $W_a$ , and where  $\theta$  and  $\phi$  are the tilt and azimuth angles at either surface ( $z = \pm d/2$ ). The following conditions (Ref. [17], Chap. 2) must be satisfied at the boundaries to minimize the total energy [in addition to bulk equilibrium equations given by Eq. (6)]:

$$\frac{\partial(\omega_F + \omega_{elec})}{\partial \theta_z} \pm \frac{\partial \omega_s}{\partial \theta} = 0, \quad (22a)$$

$$\frac{\partial \omega_s}{\partial \phi} = 0, \quad z = \pm d/2. \quad (22b)$$

The *first case* considered here is that of weak anchoring at both surface boundaries, and the following equilibrium relation for  $\phi$  at  $z = \pm d/2$  results:

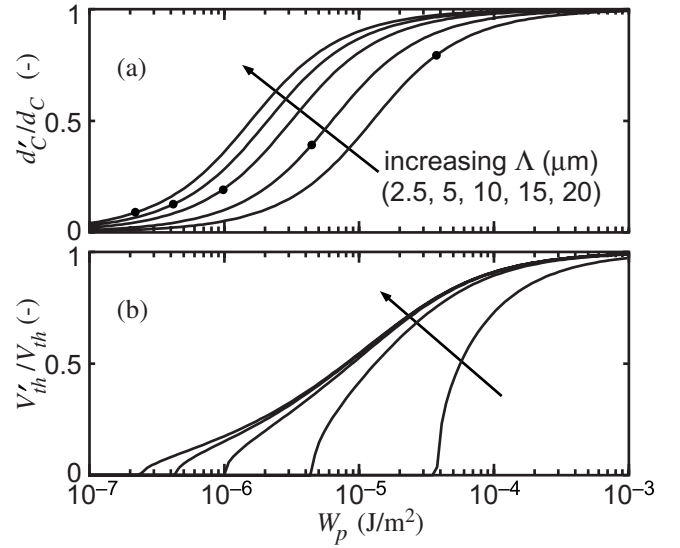


FIG. 6. (a) Weak-anchoring critical thickness  $d'_C$  and (b) voltage threshold  $V'_{th}$  dependence on polar anchoring strength  $W_p$  predicted by Eqs. (24) and (25), for various periods  $\Lambda$ . The plots are normalized to unprimed quantities  $d_C$  and  $V_{th}$  (the strong anchoring thresholds). The solid circles in (a) show the point on each curve where  $d'_C=2 \mu\text{m}$ , the thickness used for the calculation in (b).

$$W_a \cos^2 \theta \sin\left(\phi - \frac{\pi x}{\Lambda}\right) \cos\left(\phi - \frac{\pi x}{\Lambda}\right) = 0. \quad (23)$$

If  $W_a \neq 0$ , then  $\phi = \pi x / \Lambda$  minimizes this expression regardless of  $W_a$ , suggesting that azimuthal anchoring does not have a strong influence. However, analytic expressions including the polar anchoring strength can be found if we assume a one-constant approximation and follow Secs. II and III. The weak anchoring critical thickness  $d'_C$  and voltage threshold  $V'_{th}$  can be derived as

$$d'_C = \Lambda \left[ 1 - \frac{2}{\pi} \tan^{-1}\left(\frac{K\pi}{W_p \Lambda}\right) \right], \quad (24)$$

$$V'_{th} = \pi \sqrt{\frac{K}{\epsilon_0 \Delta \epsilon} \left[ \left(1 - \frac{2}{\pi} \beta_0\right)^2 - \left(\frac{d}{\Lambda}\right)^2 \right]^{1/2}}, \quad (25a)$$

$$\tan \beta_0 = \frac{K}{W_p} \left[ \frac{(V'_{th})^2 \epsilon_0 \Delta \epsilon}{d^2 K} + \left(\frac{\pi}{\Lambda}\right)^2 \right]^{1/2}. \quad (25b)$$

The prime is used here to distinguish from the strong anchoring case. The unprimed quantities are for the strong anchoring ( $W_p = \infty$ ). Note that Eqs. (25) must be solved iteratively, and that  $\beta_0$  here is the limit of Eq. (10c) evaluated at the boundaries as the tilt angles go to zero.

The predicted thresholds  $d'_C$  and  $V'_{th}$  are plotted in Fig. 6 for various grating periods, using the representative values  $d=2 \mu\text{m}$ ,  $K=10 \text{ pN}$ , and  $\Delta \epsilon=7.2$ . To clarify the effect of a finite  $W_p$ , normalized values have been plotted to show their deviation from the strong anchoring case. Two trends are important to note. First, the normalized quantities approach unity for high anchoring strengths ( $\approx W_p \geq 10^{-4} \text{ J/m}^2$ ), as expected. Second, both  $d'_C$  and  $V'_{th}$  are reduced dramatically

(ultimately to zero) even for modest anchoring strengths ( $10^{-7} \leq W_p \leq 10^{-4} \text{ J/m}^2$ ) depending on the grating period. These trends therefore suggest the thresholds will always be lower than those in the strong anchoring case and are most sensitive to the polar anchoring strength. The anchoring strength itself arises from the interaction between the alignment layer and LC [28] (influenced by both chemistry and processing), and measurements have shown that photoalignment [23,29] and rubbed polyimide [21] materials can have values within the entire range from weak ( $< 10^{-4} \text{ J/m}^2$ ) to strong ( $\approx 10^{-3} \text{ J/m}^2$ ).

An important implication from this weak anchoring analysis is now apparent. Since the actual thickness  $d$  for a device is usually determined by optical considerations [7] (e.g.  $d = \lambda/2/\Delta n \approx 2-3 \text{ }\mu\text{m}$  for visible wavelengths), it is a fixed design constraint. This design value for  $d$  will ultimately determine the minimum grating period possible, since LCPG devices must be constructed such that  $d < d_C$  in order to have in-plane anchoring, a nonzero voltage threshold, and noninfinite switching times. From Fig. 6(b), it is apparent that  $V_{th}$  goes to zero exactly when  $d = d_C$  [as indicated in Fig. 6(a) by the solid circles]. Therefore a minimum value of  $W_p$  must be implemented in order to obtain a well-aligned LCPG for a given  $d$ , and this minimum required  $W_p$  becomes more stringent as the ratio  $d/\Lambda$  approaches unity. The end result is that larger grating periods ( $> 10 \text{ }\mu\text{m}$ ) are easier to fabricate than smaller periods precisely because photoalignment materials often have modest anchoring strengths.

The *second case* of interest is that of weak anchoring on one substrate and strong anchoring at the other. This may be the best description of spin-cast reactive mesogen LCPG films [10,25], and certain switchable LCPG configurations. Since only one of the signs in the  $\pm$  terms of Eqs. (22) applies, it is possible to show that  $d'_C$  and  $V'_{th}$  for this case have the same form as before, with the change that  $2/\pi \rightarrow 1/\pi$  in Eqs. (24) and (25a). Notice that the mixed weak or strong anchoring again reduces both parameters, but in this case  $d'_C$  converges to  $\Lambda/2$  as  $W_p \rightarrow 0$ . It is important to note that if we had assumed degenerate planar anchoring ( $W_a = 0$ ) [27], we arrive at this same behavior.

From the analysis in this section, we see that the best photoalignment material for use in LCPG devices will provide strong polar anchoring. At smaller grating periods, weak anchoring effects are more pronounced and hence the choice of alignment materials becomes crucial.

## VI. COMPARISON WITH EXPERIMENT

It is now clear that the electro-optic properties of the LCPG are strongly influenced by both material properties and pixel geometry. In the strong anchoring case, the critical thickness is always less than the grating period (due to non-equal elastic constants) and the voltage threshold approaches zero as  $d$  approaches  $d_C$  (and not  $\Lambda$  as previously estimated).

It is also clear that weak anchoring can further reduce both parameters substantially, depending on both the anchoring strength and  $d/\Lambda$ .

A brief comparison of the analytic expressions derived here with experimental data is in order. Early attempts to fabricate the LCPG structure [1,25,26] resulted in strong incoherent scattering and very low diffraction. Since these works were dominated by defects, the ideal LCPG structure (Fig. 1) was not created over an appreciable area, making a comparison to the analytic expressions for the ideal case questionable. Therefore we instead compare to experimental results in more recent work [7,12–14] wherein the LCPG texture has been realized without defects and exhibits ideal optical properties ( $\sim 100\%$  diffraction efficiency and 600:1 contrast ratio).

Data from two contrasting samples with the following parameters is particularly relevant: (A) material MLC-6080,  $d = 2 \text{ }\mu\text{m}$ ,  $\Lambda = 11 \text{ }\mu\text{m}$ ; and (B) material MLC-12100-000,  $d = 2.9 \text{ }\mu\text{m}$ ,  $\Lambda = 6.3 \text{ }\mu\text{m}$ . Their measured voltage thresholds ( $V_{th} = 1.6 \pm 0.1$  and  $0.7 \pm 0.1 \text{ V}$ , respectively) are close to those predicted by Eq. (13) with  $\alpha = 0.4$ : ( $V_{th} = 1.5$  and  $1.0 \text{ V}$ , respectively). As designed, the thickness of each is below their respective critical threshold [ $d_C = 8.5$  and  $5.2 \text{ }\mu\text{m}$ , predicted by Eq. (11)]. For sample (A), all  $\alpha$  values predict a  $V_{th}$  within the measurement error, since  $d/\Lambda = 0.18$  (see Fig. 3). For sample (B), the best fit ( $\alpha = 0$ ) predicts  $V_{th} = 0.96 \text{ V}$ . However, we presume this discrepancy is linked to weak anchoring [since  $d/\Lambda = 0.46$ , see Fig. 6(b)].

The largest discrepancy we notice is with regard to the dynamics. The measured fall times were approximately constant ( $t_{off} = 1.5 \pm 0.2$  and  $8.7 \pm 0.2 \text{ ms}$ , respectively). The analytic prediction [Eq. (18b)] is a factor of  $\approx 5$  slower ( $t_{off} = 10$  and  $44 \text{ ms}$ , respectively). This effect is similar to that observed with the twisted nematic pi-cell [30] and other characteristic modes [17,21], where fluid-flow considerably accelerates director reorientation both when voltage is applied and when removed, leading to a major reduction in the switching times.

## VII. CONCLUSION

We have analyzed the equilibrium and dynamic electro-optic behavior of the LCPG profile using elastic continuum principles. Analytic expressions were derived for the critical thickness, voltage threshold, and no-flow switching times (for arbitrary elastic constants, zero pretilt, and strong anchoring). We also found that LCPGs with a small, nonzero pretilt are well characterized by the zero pretilt parameters. By comparison with experimental data, we have identified that backflow and kickback are likely prominent in the LCPG configuration, leading to faster dynamics. Numerical simulations using LC3D confirmed the validity of all these strong anchoring expressions. Finally, we derived analytic expressions that predict the influence of weak anchoring on the critical thickness and voltage threshold, and discuss its

influence on experimental LCPG realization. Because this analysis has been done within a more general framework than all previous LCPG studies, it serves as a robust guide for material optimization and device design, and the  $\alpha$  approximation is likely useful for many problems with nano- or micropatterned surfaces.

#### ACKNOWLEDGMENT

We gratefully acknowledge support from National Science Foundation Grants No. IIP-0539552 and No. ECCS-0621906.

- 
- [1] J. N. Eakin, Y. Xie, R. A. Pelcovits, M. D. Radcliffe, and G. P. Crawford, *Appl. Phys. Lett.* **85**, 1671 (2004).
- [2] H. Sarkissian, J. B. Park, B. Y. Zeldovich, and N. V. Tabirian, *Proceedings of CLEO/QELS*, 2005, p. JThE12.
- [3] L. Nikolova and T. Todorov, *Opt. Acta* **31**, 579 (1984).
- [4] F. Gori, *Opt. Lett.* **24**, 584 (1999).
- [5] J. Tervo and J. Turunen, *Opt. Lett.* **25**, 785 (2000).
- [6] W. M. Jones, B. L. Conover, and M. J. Escuti, *SID Int. Symp. Digest Tech. Papers* **37**, 1015 (2006).
- [7] M. J. Escuti and W. M. Jones, *Proc. SPIE* **6332**, 63320M (2006).
- [8] T. Todorov, L. Nikolova, K. Stoyanova, and N. Tomova, *Appl. Opt.* **24**, 785 (1985).
- [9] S. Slussarenko, O. Francescangeli, F. Simoni, and Y. Reznikov, *Appl. Phys. Lett.* **71**, 3613 (1997).
- [10] M. J. Escuti, C. Oh, C. Sanchez, C. W. M. Bastiaansen, and D. J. Broer, *Proc. SPIE* **6302**, 632614 (2006).
- [11] G. Cipparrone, A. Mazulla, and L. Blinov, *J. Opt. Soc. Am. B* **19**, 1157 (2002).
- [12] M. J. Escuti and W. M. Jones, *SID Int. Symp. Digest Tech. Papers* **37**, 1443 (2006).
- [13] W. M. Jones, C. Oh, R. Komanduri, and M. J. Escuti, in *International Display Research Conference*, 2006, Vol. 26, p. 12.5.
- [14] R. K. Komanduri, W. M. Jones, C. Oh, and M. J. Escuti, *J. Soc. Inf. Disp.* **15**, 589 (2007).
- [15] H. Sarkissian, N. Tabirian, B. Park, and B. Zeldovich, *Storming Media Report No. A000824*, 2004.
- [16] C. Oh, R. Komanduri, and M. J. Escuti, *SID Int. Symp. Digest Tech. Papers* **37**, 844 (2006).
- [17] I. W. Stewart, *The Static and Dynamic Continuum Theory of Liquid Crystals* (Taylor & Francis, London, 2004).
- [18] S. Chandrasekhar, *Liquid Crystals* (Cambridge University Press, New York, 1992).
- [19] J. E. Anderson, P. E. Watson, and P. Bos, *LC3D [computer file]: Liquid Crystal Display 3-D Director Simulator Software* (Artech House Publishers, Norwood, 2001).
- [20] Merck technical datasheet (provided upon request), 2005.
- [21] K. Takatoh, M. Hasegawa, M. Koden, N. Itoh, R. Hasegawa, and M. Sakamoto, *Alignment Technologies and Applications of Liquid Crystal Devices* (Taylor & Francis, New York, 2005).
- [22] P. Yeh and C. Gu, *Optics of Liquid Crystal Displays* (Wiley, New York, 1999).
- [23] H. S. Kwok, V. G. Chigrinov, H. Takada, and H. Takatsu, *J. Disp. Technol.* **1**, 41 (2005).
- [24] V. Chigrinov, A. Muravski, and H. S. Kwok, *Phys. Rev. E* **68**, 061702 (2003).
- [25] G. P. Crawford, J. N. Eakin, M. D. Radcliffe, A. C. Jones, and R. A. Pelcovits, *J. Appl. Phys.* **98**, 123102 (2005).
- [26] H. Sarkissian, S. V. Serak, N. V. Tabirian, L. B. Glebov, V. Rotar, and B. Y. Zeldovich, *Opt. Lett.* **31**, 2248 (2006).
- [27] W. Zhao, C. X. Wu, and M. Iwamoto, *Phys. Rev. E* **65**, 031709 (2002).
- [28] J. Hoogboom, T. Rasing, A. E. Rowan, and R. J. M. Nolte, *J. Mater. Chem.* **16**, 1305 (2006).
- [29] M. Vilfan, I. D. Olenik, A. Mertelj, and M. Copic, *Phys. Rev. E* **63**, 061709 (2001).
- [30] S. H. Chen and C. L. Yang, *Appl. Phys. Lett.* **80**, 3721 (2002).